High-Field EPR Study of Frozen Aqueous Solutions of Iron(III) Citrate Complexes

Frédéric Biaso,[a] Carole Duboc,[b] Bernard Barbara,[c] Guy Serratrice,[a] Fabrice Thomas,[a] Denis Charapoff,[a] and Claude Béguin*[a]

Keywords: High-field EPR spectroscopy / Iron / Coordination chemistry / Citrate ligand / Tripodal ligand / Spin crossover

High-field electron paramagnetic resonance spectra have been measured for frozen aqueous solutions of Fe^{III} citrate at acidic and neutral pH values. At high fields (up to 12 T) and high frequencies (95, 190 and 285 GHz), fine-structure peaks due to resonance between Kramers doublets (±1/2, ±3/2, ±5/2) of an $S = 5/2$ species can be observed when the experiments are performed at high temperatures. A full-matrix diagonalisation approach has been used to derive the spin-Hamiltonian parameters for the $S = 5/2$ spin state. In acidic media (pH = 2), the spacing of the fine structure reveals that the value of the axial zero-field splitting (ZFS) parameter D is -0.12 cm^{-1} without rhombicity. A small but significant g anisotropy can be observed which depends slightly on the frequency and the temperature ($g_x = 2.014$, $g_y = 2.014$ and $g_z = 1.983$, at 60 K and 285 GHz). In neutral media (pH = 6), complete rhombic HF-EPR spectra were observed with a fivefold lower $|D|$ value (0.024 cm^{-1}) and $E = 0.008$ cm^{-1}. A satisfactory simulation of the experimental data was obtained with a g value equal to 2.00. The different ZFS parameters obtained under neutral and acidic conditions are discussed in terms of the symmetry of the complex. At low temperatures, a spin transition from 5/2 to 1/2 occurs at all frequencies. The transition temperature is pH- and field-dependent. A model including magnetoelasticity has been suggested in order to interpret the field dependency of the spin transition observed for the two systems.

Introduction

Citric acid is widely known for its abundance in biological fluids and plays key roles in the biochemical processes of bacteria, plants, animals and humans. Its structure, with three carboxylate groups and one hydroxy group, bestows on it unique chemical properties which render it essential in biological media.[1] Besides participation in the Krebs cycle[2] and acting as a component in a number of metalloenzyme active sites,[3] citric acid is a target ligand of a large number of trace metal ions found in biological fluids. Its chelating ability, exemplified in a multitude of coordination modes, plays an important role in metal solubilisation, mobilisation and bioavailability in biological media.[1,4] Among these metal ions, we have a particular interest in ferric ions.[5−7] In humans, citrate is present in blood plasma at a concentration of about 0.1 mM and is believed to be one of the major components of nontransferrin-bound iron (NTBI).[8a,9] It has been proposed that NTBI in the plasma of iron-overloaded patients exists largely in the form of complexes with citrate.[10] Citrate has also been proposed as a component of the cytosolic (or intracellular) iron pool known as the "Labile Iron Pool" (LIP). Other ligands involved in the LIP (which is also called the chelatable pool, transit pool or low molecular weight iron pool) could be AMP, ATP, pyrophosphate, amino acids or nucleoside phosphates.[8b,11] In vivo approaches have been developed to obtain information about the concentration and the nature of this LIP.[8] For a correct interpretation of the biological processes related to the Fe^{III} citrate system, it is necessary to obtain more insight, using noninvasive approaches, into the nature of the chemical species of this system present in aqueous solutions. The dependence of the system on the experimental conditions (stoichiometry, solvent, pH, added ligand or bases etc.) could therefore be easily studied.

High field electron paramagnetic resonance (HF-EPR) experiments performed on aqueous solutions of Fe^{III} citrate should be a good in vitro noninvasive approach. At high frequencies (95, 190 and 285 GHz, i.e. high energy radiation of ca. 3−10 cm^{-1}) and high fields (up to 12 T), we could directly observe EPR resonances between the energy levels. The splitting of these levels depends on the Zero-Field Splitting (ZFS) parameters (Kramers doublets) and on the Zeeman effect. At high fields, the Zeeman interaction is

[a] Institut de Chimie Moléculaire de Grenoble, Laboratoire de Chimie Biomimétique, LEDSS, UMR-CNRS 5616, Université Joseph Fourier,
B. P. 53, 38041 Grenoble, Cedex 9, France
Fax: (internat.) + 33-4-76514836
E-mail: Claude.Beguin@ujf-grenoble.fr
[b] High Magnetic Field Laboratory of Grenoble, HMFL, CNRS-MPI UPR 5021,
B. P. 166, 38042 Grenoble, Cedex 9, France
[c] Laboratoire Louis Néel, CNRS-LLN UPR 5051,
B. P. 166, 38042 Grenoble, Cedex 9, France
Supporting information for this article is available on the WWW under http://www.eurjic.org or from the author.

dominant compared with the ZFS interaction. As a consequence, the ZFS parameters could be determined much more precisely than with conventional X-band EPR spectroscopy (9.4 GHz).[12] By performing measurements at high frequencies, the resonance positions of a Kramer transition may be tracked in order to determine the anisotropy of the *g* tensor even if it is weak (ranging between 1.950 and 2.040 in our case). This might lead to a considerably improved understanding of the symmetries and electronic structures of these biologically relevant Fe^{III} complexes.

The major aim of this study was to measure the ZFS parameters of mononuclear Fe^{III} citrate complexes in aqueous solutions and to find a correlation between the ZFS and the geometry around the iron. Another aim was to confirm, for these experimental conditions, the mononuclear structures of these complexes since the reported coordination chemistry of ferric citrate remains sketchy.[8] The complexes were obtained from solutions where citrate was in excess of the ferric ions (20:1 as respective molar ratio) at two different pH levels. We studied the anions **1** (at pH = 1.95) and **2** (at pH = 6.2) with Na^+ as the counterion. The protonation states of these chemical species cannot be obtained by UV/Vis spectrophotometry or by potentiometric titration. We believe, however, from comparisons with literature data (vide infra), that the structure of **1** is $[Fe(HCit)(H_2Cit)]^{2-}$. Complex **2** has been previously identified using electrospray mass spectrometry as having the structure $[Fe(HCit)(Cit)]^{4-}$ and this was confirmed by X-ray analysis (where Cit is the completely deprotonated citric acid) as shown in Figure 1.[13]

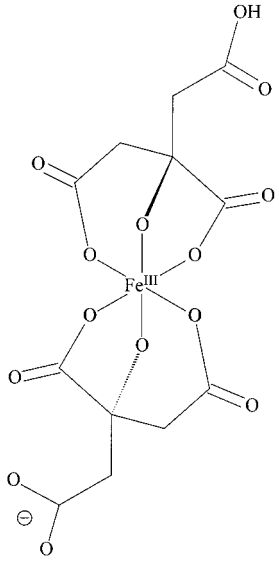

Figure 1. Schematic representation of the anion $[Fe(HCit)(Cit)]^{3-}$

Results

1. High-Field EPR Spectra of 1 and 2 at 60K

The 60 K HF-EPR spectra of **1** and **2**, at frequencies ranging between 95 and 285 GHz, are shown in Figures 2 and 3, respectively. They have been simulated using the spin-Hamiltonian parameters reported in Table 1 (see Exp. Sect. for details). Compound **1** exhibits purely axial symmetry with a *D* value of $|0.12|$ cm^{-1}. The values of the Landé factor vary slightly as a function of the frequency (small increase of $g_\perp$ and small decrease of $g_{//}$ when the frequency decreases, Table 2). All the transitions are shown in Figure 2 with their interpretations using energy level diagrams (e−f in Figure 2). $\Delta M_S = 2$ transitions centred at 1.75 T for 95 GHz can also be recalculated from the energy level diagrams (see d−f in Figure 2).

The negative sign of *D* was determined by careful examination of the intensities of the transitions as a function of temperature (from 20 to 60 K). At 285 GHz, when the temperature increases, the intensities of the [5/2,1/2> to 5/2,3/2>]$_{//}$ and [5/2,1/2> to 5/2,3/2>]$_\perp$ transitions, located at 10.52 T and 9.98 T, respectively, increase, while that of the 5/2,−3/2>$_\perp$ to 5/2,−1/2>$_\perp$ transition decreases at 10.23 T. This agrees with the energy level diagram shown on the right of Figure 2.

For compound **2**, both the high field (Figure 3 and Figure SI1 in the Supporting Information; for Supporting Informations see also the footnote on the first page of this article) and X-band EPR spectra (data not shown) are rhombic. The experimental and simulated 285 GHz EPR spectra recorded at 60 K are shown in Figure 3. At this frequency, the EPR spectrum is constrained between 10.0 and 10.5 T in agreement with a magnitude of *D* five times smaller than that for compound **1** ($|D| = 0.024$ cm^{-1}, with $|E|$ equal to 0.008 cm^{-1}; $\lambda = |E/D| = 1/3$). Since the zfs tensor is completely rhombic, the sign of D has no significance. The different transitions of the $S = 5/2$ paramagnet with their interpretations using energy level diagrams are shown in the Supporting Information (SI1).

2. Evolution of the High-Field EPR Spectra of 1 and 2 as a Function of Temperature from 60 to 5 K

The 285 GHz HF-EPR spectra were found to be temperature-dependent in the 5 to 60 K range (Figure 4) for compound **1** and between 5 and 30 K for compound **2** (Figure SI2 in the Supporting Information). At 5 K, the $S = 5/2$ spectrum was not observed. Instead, an axial $S = 1/2$ signal dominates the spectra of **1** and **2**. The $S = 1/2$ spectra are characterised by a very large line width ($w_{1/2} = 0.5$ T) suggesting a much higher relaxation rate of the $S = 1/2$ species than for the $S = 5/2$ species. However, the line widths of each spin state for compounds **1** and **2** are similar at all frequencies indicating that the frequency has no effect on the relaxation rate of the different species. The $S = 1/2$ signals for compounds **1** and **2** were simulated (see Exp. Sect.) with a small *g* anisotropy in the perpendicular region of the spectra (Table 3). The differences in relaxation rates between the $S = 5/2$ and the $S = 1/2$ spectra are so high that their relative contribution to the spectra could not be precisely obtained. Therefore, it was difficult to evaluate the critical temperature (i.e. T_c, the transition temperature where the molar fractions of the two spin states are equal). However, Figure 4 and SI2 show that the spin conversion is

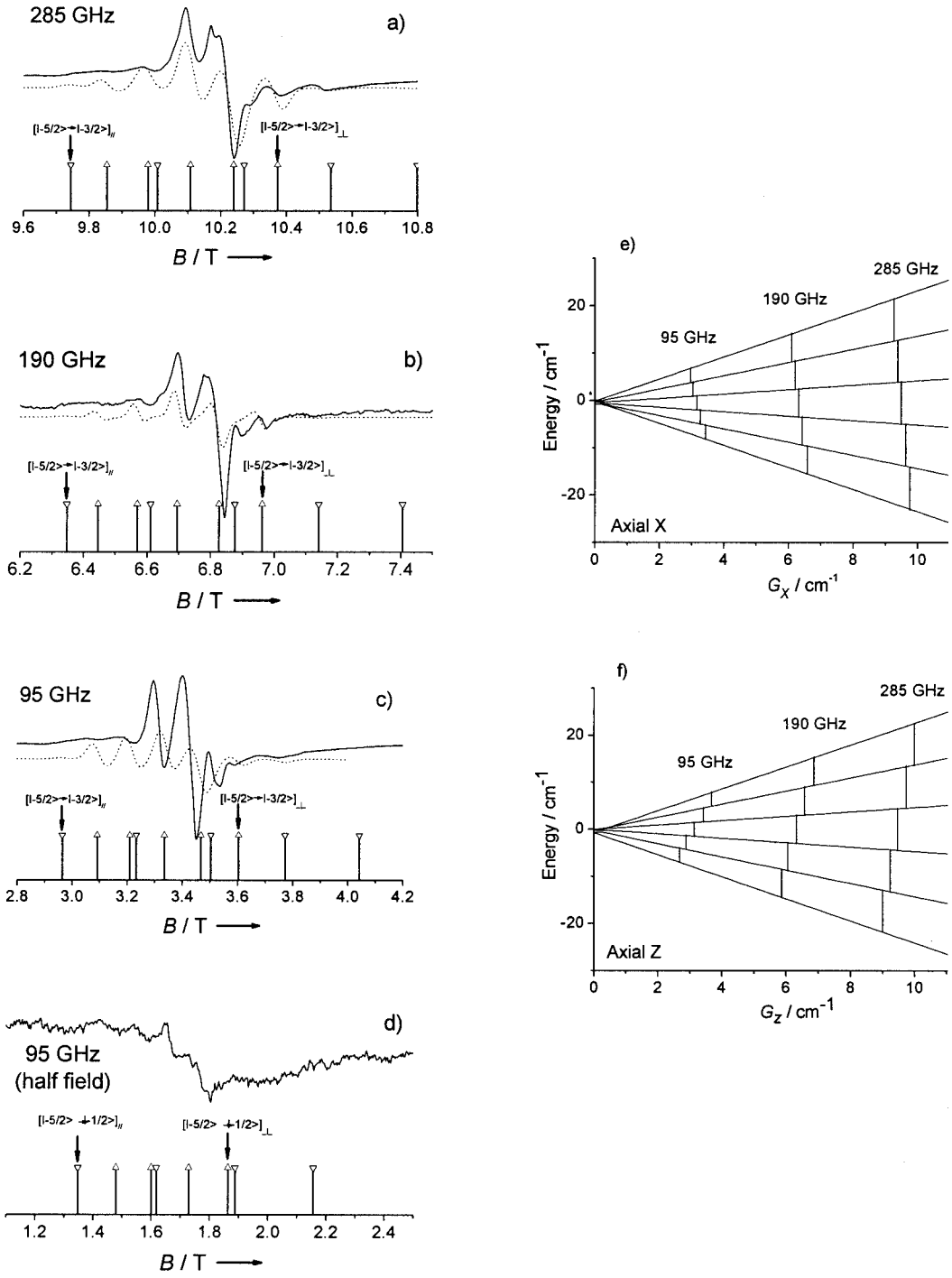

Figure 2. Experimental (bold lines) and simulated (dotted lines, with $D = -0.12$ cm^{-1} and g_x, g_y and g_z according to Table 2) HF-EPR spectra of compound **1** recorded at 60 K and at 285 (a), 190 (b) and 95 GHz (c and d); the assignments of the different transitions are represented as sticks (// parallel and ⊥ perpendicular); in the right-hand part, energy levels calculated for the axial spin-Hamiltonian (see Exp. Sect.) as a function of G_q ($g_q\beta B_o$) are shown; the expected resonances at 95, 190 and 285 GHz are indicated by vertical bars (e) for G_x and (f) for G_z

not abrupt for **1** and **2** but they do not show the presence of a hysteresis loop around T_c.

In Figure 5, the frequency dependence of the HF-EPR spectra of compound **1** is shown at 12.5 K. The $S = 5/2$ component dominates the spectrum with a minor $S = 1/2$ component at 95 GHz, whereas the reverse is true at 285 GHz with a major contribution to the spectrum from the $S = 1/2$ species. This reveals that T_c increases as the field increases. Another way to illustrate this phenomenon is to look at HF-EPR spectra recorded at different frequencies and at different temperatures which appear with similar shapes as shown in Figure 6. At the particular tem-

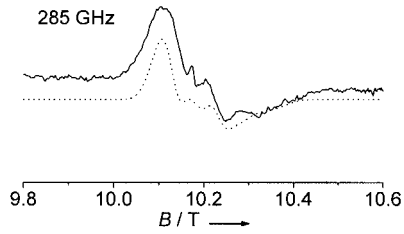

Figure 3. Experimental and simulated HF-EPR spectra for compound **2** at 60 K and at 285 GHz

peratures of 5.0, 9.0 and 12.5 K for 95, 190 and 285 GHz, respectively, the relative intensities of the signals corresponding to the two spin states appear almost equivalent. Thus, these temperatures can be an estimate of the T_c at each frequency, demonstrating that T_c increases almost linearly with the external magnetic field (Figure SI3, Supp. Inf.).

At 285 GHz, the estimate of T_c for compound **2** is much lower than for compound **1** since the $S = 5/2$ spectrum can be observed even at 5 K.

Table 1. Energy matrix of 6 × 6 elements for the $S = 5/2$ spin state characterised by a rhombic zero-field splitting with an external magnetic field B_0, oriented along the molecular axis of the complex, according to the Cartesian components B_x, B_y and B_z; the notations are $G_z = \beta g_z B_z$, $z = G_x + iG_y$ and $z^* = G_x - iG_y$ with $G_x = \beta g_x B_x$ and $G_y = \beta g_y B_y$; all parameters (D, E, G_x, G_y and G_z) have to be treated with the same energy unit (cm^{-1})

M_s	|+5/2>	|+3/2>	|+1/2>	|−1/2>	|−3/2>	|−5/2>
<+5/2|	$10/3D + 5/2G_z$	$\sqrt{5/2}\ z^*$	$\sqrt{10}\ E$	0	0	0
<+3/2|	$\sqrt{5/2}\ z$	$-2/3D + 3/2G_z$	$\sqrt{2}\ z^*$	$3\sqrt{2}\ E$	0	0
<+1/2|	$\sqrt{10}\ E$	$\sqrt{2}\ z$	$-8/3D + 1/2G_z$	$3/2\ z^*$	$3\sqrt{2}\ E$	0
<−1/2|	0	$3\sqrt{2}\ E$	$3/2\ z$	$-8/3D - {}^1/_2G_z$	$\sqrt{2}\ z^*$	$\sqrt{10}\ E$
<−3/2|	0	0	$3\sqrt{2}\ E$	$\sqrt{2}\ z$	$-2/3D - 3/2G_z$	$\sqrt{5/2}\ z^*$
<−5/2|	0	0	0	$\sqrt{10}\ E$	$\sqrt{5/2}\ z$	$10/3D - 5/2G_z$

Table 2. ZFS parameters and g factors of the high-spin Fe^{III} complexes **1** (pH = 2.0) and **2** (pH = 6.2) at 60 K

pH	Frequency [GHz]	D [cm^{-1}]	E [cm^{-1}]	λ	g_x	g_y	g_z
2.0	285	− 0.122	0	0	2.014	2.014	1.983
2.0	190	− 0.122	0	0	2.026	2.026	1.975
2.0	95	− 0.122	0	0	2.030	2.030	1.939
6.2	285	± 0.024	0.008	0.33	2.015	1.990	1.985

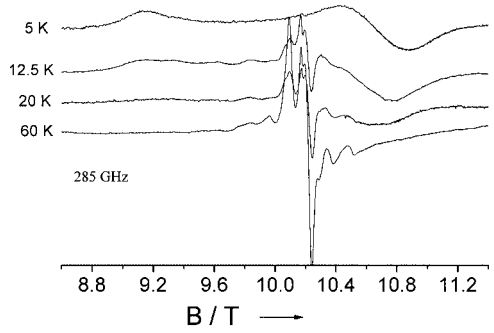

Figure 4. Experimental HF-EPR spectra of compound **1** at 285 GHz as a function of temperature (from 5 to 60 K)

Table 3. g factors of the low-spin Fe^{III} complex **1** as a function of frequency and of the low-spin Fe^{III} complex **2**

pH	Frequency [GHz]	g_x	g_y	g_z
2.0	285	1.850	1.915	2.370
2.0	190	1.875	1.915	2.225
6.2	285	1.870	1.910	2.245

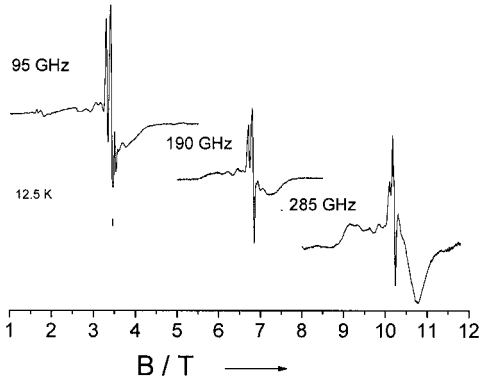

Figure 5. Experimental HF-EPR spectra of compound **1** at 12.5 K as a function of frequency (95, 190 and 285 GHz)

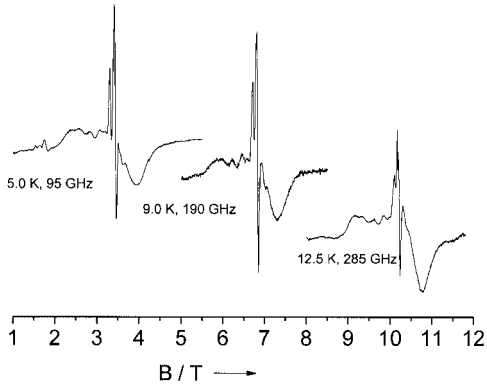

Figure 6. Experimental HF-EPR spectra of compound **1** at 95 GHz (5 K), 190 GHz (9 K) and 285 GHz (12.5 K)

Discussion

1. Comparison of the Zero-Field Splitting Parameters with Literature Data

Values of ZFS parameters for high-spin Fe^{III} complexes have been reported in the literature only recently due to the development of high-field EPR techniques. A very early (1973!) paper by Y. Alpert et al. has indisputably been the classic in biological HF-EPR spectroscopy with measurements at various microwave frequencies in the millimetre region (called far-infra red magnetic resonance by some authors).[14] In some cases, measurements of spectra as a function of temperature give the sign of *D*. EPR measurements at X- or Q-band frequencies (with an appropriate treatment of the data), magnetic susceptibility measurements or Mössbauer experiments have also been reported as giving *D* values usually without sign determination.

In Table 4, we have gathered several *D* and λ values determined for low molecular weight mononuclear Fe^{III} complexes or metalloproteins. Absolute *D* values vary from very small up to 12 cm^{-1} while those of λ vary from 0 (complete axial symmetry) to 0.33 (complete rhombic symmetry). We discuss the data in three main groups.

(i) The first group concerns the non-heme octahedral Fe^{III} complexes. The complexes $[Fe(dpm)_3]$, $K_3[Fe(malonate)_3]$, $K_3[Fe(oxalate)_3]$, $K_3[Fe(acac)_3]$ and ferrichrome A have three bidentate ligands for which the denticity only originates from oxygen atoms.[15−18] They are characterized by small *D* values ($|D| < 0.3$ cm^{-1}). Three of these complexes exhibit a quasi-axial ZFS ($\lambda < 0.055$) while the other two show a moderate rhombicity with $\lambda \approx 0.25$. Since a discrepancy in *D* appears in the literature for ferrichrome A we retained, in Table 4, only the values extracted from HF-EPR measurements.[17,18] When nitrogen atoms are present in the coordination shell of Fe^{III}, the magnitude of *D* (0.3−1.7 cm^{-1}) increases in comparison with the values for the previous complexes. The coordination mode varies between $[N_2O_4]$,[19−22] $[N_4O_2]$[23] and $[N_5O]$.[24] EPR measure-

Table 4. ZFS parameters of compounds described in the literature with the spectroscopic method used for the measurements

Compound	*D* [cm^{-1}]	λ	Method[a]	Ref.
Octahedral iron(III)				
Molecular complex				
$Fe(citrate)_2$ pH 1.95	−0.12	0.0	HF	this work
pH 6.2	|0.024|	0.33	HF	this work
$Fe(dpm)_3$ [b]	−0.18	0.25	HF	[15]
$K_3Fe(malonate)_3$	|0.12|	0.032	X,Q	[16]
$K_3Fe(oxalate)_3$	|0.18|	0.055	X,Q	[16]
$K_3Fe(acac)_3$[c]	|0.14|	0.028	X,Q	[16]
Ferrichrome A	−0.27	0.25	HF	[17,18]
Fe^{III}-EDTA[d]	+ 0.8	0.33	HF	[19,20]
	+ 0.78	0.33	HF	[21]
	|0.83|	0.31	X	[22]
2 trispicMeen (OO)[e]	−1.7	0.0	X,Mos.	[23]
Fe bztpem[f]	|0.3|	0.15	X	[24]
Tris(dithiocarbamate)	− 2.14	0.10	HF	[17]
Protein				
Transferrin	+0.3	0.29	HF	[19,21]
	+0.27	0.31		[22]
Lipoxygenase	2	−	HF	[25]
	≈|2|	−	X,Q	[26]
Fe-SOD	−2	0.23	X	[28]
Pentacoordinated iron(III)				
Bis(dithiocarbamateFeBr)bis(dithiocarbamateFeCl)	+7	0.07	HF	[17]
	−2	0.04	HF	[17]
Schiff base (square planar)	|10| (|7.2|)	0.33 (0.33)	Magn.	[29]
Bis(substituted-thiohydroxamate)	|10|	0.3	Magn.	[30]
Heme complex				
Protoporphyrin IX-F^- (Br^-)	|5| (|11.8|)	0	FIR	[17,31]
Protohemes	|10|	0	FIR	[31]
	|7|	0	Magn.	[32]
	|6|	0	Magn.	[33]
Metmyoglobin	|10|	0	HF	[34]
	+9.5	0	HF	[17,21]
Metmyoglobin + F-	5.9, 5.0	0, 0	HF	[17,21]
Methemoglobin	|10.7|	0	FIR	[34]
Methemoglobin (F-)	+6.3	0	FIR	[17]

[a] HF: HF-EPR measurements; X,Q: EPR measurements at X or Q band frequencies; Mos: Mössbauer spectroscopy; Magn: magnetic susceptibility measurements and FIR: Far Infra-Red spectroscopy. [b] dpm: dipivaloylmethane. [c] acac: pentane-2,4-dionate. [d] EDTA: ethylenediaminetetraacetate. [e] trispicMeen: *N*-methyl-*N*,*N*′,*N*′-tris(pyridylmethyl)ethane-1,2-diamine. [f] bztpem: *N*-benzyl-*N*,*N*,*N*′,*N*′-tetrakis(pyridylmethyl)ethane-1,2-diamine.

ments performed at several high frequencies are well documented for the Fe^{III}-EDTA complex.[21] For all these octahedral complexes, the $|D|$ values increase as a function of the nature of the coordinating atoms in the order: $[O_6] < [N_2O_4] < [N_4O_2] < [N_5O] < [S_6]$. Among the non-heme proteins, only three iron sites have been studied and the magnitude of D is < 3 cm^{-1}. In the case of transferrin, rhombic spectra have been correlated with the distorted octahedral structure found in the enzyme.[19−21] The iron is coordinated by four monodentate amino acid residues and one bidentate carbonate anion giving an $[NO_5]$ set of donor atoms.[8c] For lipoxygenase, EPR measurements both at low (X band) and high frequencies have been made and give the same magnitude of D (sign determined at high frequencies).[25−26] The corresponding structural data show an $[N_3O_3]$ coordination mode.[27] In the case of the bacterial Fe-superoxide dismutase (Fe-SOD), attention must be drawn to the detailed X-band EPR study. From a precise temperature-dependent spectroscopic analysis, the magnitude and sign of D were obtained.[28] The observed rhombicity ($\lambda = 0.23$) can be explained in relation to the X ray structure of the Fe-SOD from *E. coli* which reveals that the active site is a pentacoordinate complex. The iron atom is coordinated by three histidines, one aspartate and a hydroxide anion resulting in a distorted structure.

(ii) The second group concerns Fe^{III} complexes characterised by a C_{4v} geometry in the coordination sphere. All of these complexes possess halogen ligands. The magnitude of D varies in a large range (2 to 10 cm^{-1}) and has been correlated with the nature of the halogen ligand. For instance, D increases from -2 to $+7$ cm^{-1} when the chloride ligand is replaced by a bromide ligand in $[(R_2NCS_2)_2FeX]$ [R_2NCS_2 is a bis(dithiocarbamate)].[17] The other chloro iron complex [chlorobis(*N*-methylbenzothiohydroamato)Fe^{III}] is characterised by a larger D value (between 7 and 10 cm^{-1}).[29−30] From the X-ray structures determined for several complexes, the magnitude of D can be correlated with the distance between the iron ion and the plane formed by the four equatorial ligands along the axis formed by the fifth ligand and the metal atom. $|D|$ increases when the distances become smaller.

(iii) The third group concerns the (heme)Fe^{III} complexes such as (porphyrin)Fe^{III} and (protein)Fe^{III} complexes such as metmyoglobin and hemoglobin.[14,17,21,31−34] The systematic axial symmetry originates from the conjugated electronic structure of the haeme. When the metal atom lies in the heminic plane, the D values are in the range of 9 to 12 cm^{-1}.[14,17,31−34] On the other hand, when the iron atom lies above the heme plane, the D values become smaller, between 5 and 10 cm^{-1}.[14,17,31−34] The shift of the iron atom above the plane occurs when an additional ligand coordinates to the iron site giving a sixth coordination site. Recently, the sign of D was clearly obtained as being positive for metmyoglobin.[21]

In conclusion, compounds **1** and **2** can be compared with the non-heme octahedral complexes. The D value of 0.12 cm^1 determined for **1** is in the range found for complexes characterised by a $[O_6]$ coordination sphere ($0.12 < D <$ 0.28 cm^1). For compound **2**, the D value of 0.024 cm^{-1} is smaller but can be closely compared with the other complexes extending the previous range. However, all these D values are smaller than those of the other octahedral complexes in which the coordination spheres contain other heteroatoms as for the EDTA complex ($[N_2O_4]$) with $D = 0.8$ cm^{-1}. In our case, the pH change between compounds **1** and **2** leads to a drastic evolution of λ from a purely axial to a totally rhombic system.

2. Zero-Field Splitting Parameters and Structures of Compounds 1 and 2

It is interesting to compare the ZFS parameters with structural data. Different chemical species have been identified in aqueous solutions depending on the pH. In solutions containing 1 μM Fe^{3+} and 0.1 mM citrate at pH = 5−6, $[Fe(citH)_2]^{3-}$ and $[Fe(cit)]^-$ were observed.[35] More recently, different complexes formed from Fe^{III} and citric acid in the pH range 1−13 have been studied by magnetic susceptibility measurements.[36]

The crystal structures of several mononuclear dicitrate complexes with metal(III) ions, with different degrees of protonation, have been obtained in our laboratory. From these results, we should be able to suggest likely structures for compounds **1** and **2**.

At pH = 7, $(NH_4)_5[Fe(Cit)_2]\cdot 2H_2O$ was isolated.[13] The structure is centrosymmetric with the Fe^{III} ion located on an inversion centre. The coordinated oxygen atoms with the similar chemical functions of each citrate are in *trans* positions. This coordination mode involves the formation of a seven-, a six- and a five-membered coordination ring. The remaining terminal carboxylates are noncoordinating. These results are in agreement with those reported in the literature at almost the same pH.[37] The shortest Fe−O bond is 1.942 Å for the Fe−O (alkoxide) bond. The other distances are 1.995 Å for the Fe−O (central carboxylate) bond and 2.055 Å for the Fe−O (terminal carboxylate) bonds.[13]

At pH = 6, single crystals of $(NH_4)_4[Fe(HCit)(Cit)]\cdot 3H_2O$ were isolated.[13] Since the protonation state of each ligand is different, the Fe^{III} ion is no longer located on an inversion centre thus inducing a pseudo-centrosymmetrical complex. The proton in the (Hcit) ligand is located on the pendant terminal carboxylic acid. The Fe−O bond lengths are nevertheless in the same range as those of the previous complex $(NH_4)_5[Fe(Cit)_2]\cdot 2H_2O$. The values of the Fe−O bond lengths are: 1.932 and 1.944 Å for the Fe−O (alkoxide) bonds, 2.007 and 2.019 Å for the Fe−O (central carboxylate) bonds, and 2.035 Å and 2.064 Å for the Fe−O (terminal carboxylate) bonds, for the nonprotonated and protonated ligands in each case, respectively. No crystals could be obtained at other acidic pH values.

Crystal structures of related complexes found in the literature give an idea of the structure of compound **1**. The structure of $(NH_4)_4[Fe(HCit)(Cit)]\cdot 3H_2O$ is isostructural with $(NH_4)_4[Al(HCit)(Cit)]\cdot 3H_2O$ and $(NH_4)_4[Ga(HCit)(Cit)]\cdot 3H_2O$ which have been previously characterised.[38]

The Ga−O bond lengths are 1.893 and 1.900 Å for the Ga−O (alkoxide) bonds, 1.976 and 1.983 Å for the Ga−O (central carboxylate) bonds, and 2.022 and 2.058 Å for the Ga−O (terminal carboxylate) bonds, for the nonprotonated and protonated ligand in each case, respectively. The $[Ga(HCit)(H_2Cit)]^{2-}$ species was recently characterised in the laboratory at pH = 1.5.[39] This complex has two pendant terminal carboxylic acid functions and the Ga^{III} centre is linked to an alkoxide oxygen atom for the monoprotonated ligand and an alcoholic oxygen atom for the diprotonated ligand. The Ga−O bond lengths are 1.878 Å for the Ga−O (alkoxide) bond and 2.038 Å for the Ga−O (alcoholic) bond, the other distances are 1.945 and 1.936 Å for the Ga−O (central carboxylate) bonds, and 2.013 and 2.003 Å for the Ga−O (terminal carboxylate) bonds. These results unambiguously demonstrate that protonation of the alkoxide oxygen increases the Ga−O bond distance.

We therefore suggest that the geometry of compound **2** is strongly related to that of $(NH_4)_4[Fe(HCit)(Cit)]\cdot 3H_2O$. The only difference comes from the difference in the counterion (Na^+ instead of NH_4^+). All of the Fe−O bonds distances are in the range of 1.932 to 2.035 Å, within an interval of 0.1 Å suggesting a rhombic octahedral geometry around the Fe^{III} ion. Although the geometry of compound **1** is still unknown, a comparison of isostructural Ga^{III} and Fe^{III} citrates with different degrees of protonation suggests that the protonation of one or two alcoholic oxygen atoms increases the Fe−O (alcoholic) bond distances leading to an axial octahedron with a long O(alcoholic)−Fe−O(alcoholic) axis. This change of structure related to the variation in the acidity of the medium can therefore be correlated with the strong evolution of the ZFS parameters, extracted from the high-field EPR spectra, when the pH of the medium shifts from 6 to 2.

3. Spin Crossover in 1 and 2

All of our results suggest that complexes **1** and **2** are mononuclear, and we will attempt to explain the different phenomena that we observed starting with the following hypothesis.

We therefore exclude to interpret our data on the basis of two different spin states originating from a trinuclear high-spin Fe^{III} complex. For instance, in the literature, the $[Fe_3S_4]^+$ sites of ferredoxins were characterised by an S = 1/2 ground state and an S = 5/2 excited state. The spin ground state S = 5/2 or S = 1/2 depends on the magnitude of the different antiferromagnetic exchange couplings between the three iron sites.[40] Nevertheless, it has been found by Girerd et al., that in a certain temperature range, an S = 3/2 species becomes stabilised for such trinuclear iron−sulfur complexes. In our case, no evidence of an S = 3/2 spectrum arising from a trinuclear Fe^{III} complex has been found in our experimental data.

Moreover, the observation of such a spin crossover for our $[O_6]$-coordinated iron(III) complexes was quite unpredictable.[41] Indeed, no critical temperature of a spin transition has been described for such compounds. Nevertheless, a spin transition has been established for an iron(III)-substituted acac complex by magnetic moment measurements.[42] From a general point of view, iron(III) spin-crossover compounds are less common than those of iron(II).[41,43] However, early studies on tris(dithiocarbamato)iron(III) complexes $[Fe(S_2CNRR')_3]$ indicated that, depending on the nature of R and R′, the iron(III) is high or low spin or spin crossover in this $[S_6]$ coordination sphere.[41,44] In the case of porphyrinic systems, including ferric haemo proteins, characterised by a $[N_4L_2]$ coordination sphere, spin crossover has been observed (L represents different types of monodentate ligands).[41,45] The origin of this phenomenon has been related to a spin state stereochemical relationship. Spin crossover has also been seen for complexes with $[N_6]$ and $[N_4O_2]$ coordination spheres.[46−47]

Spin Transition Equilibrium and Critical Temperature T_c

At 5 K, the 1/2 spin state corresponds to the major species in solution. When the temperature is increased, the S = 5/2 species appears at the expense of the 1/2 species (Figure 4). Since the relaxation properties of the two species differ strongly, it is difficult to evaluate the critical temperature T_c. Comparing the relative appearance of the two spectra it is possible, however, to characterise the variation of these T_c values as a function of the nature of the complex and the field (see below). For instance, at 285 GHz, T_c is smaller for the complex in a neutral medium ($T_c < 10$ K) than it is under acidic conditions (T_c = 12.5 K) (Figure 4 and SI2, Supp. Inf.). For the compounds **1** and **2**, their T_c values are, by far, smaller than that those already found in the literature for Fe^{III} complexes with $[S_6]$, $[N_6]$ or $[N_4O_2]$ coordination shells. For these last compounds, the T_c values are in the range from room temperature to 70 K.[41]

The experimental data are reproducible even if measurements are performed by increasing or decreasing the temperature, implying that no hysteresis phenomena occur. Thus, we have interpreted the presence of these two paramagnetic species as a thermal spin transition (or spin-crossover) of a unique chemical species changing from the 1/2 spin state to the 5/2 spin state according to the following equilibrium:

$$LS\ (^2T_2) \rightleftarrows HS\ (^6A_1)$$

The spin-state interconversion seems to be "prepared" below T_c. Indeed, the evolution of the g anisotropy of the S = 1/2 species with temperature (seen at 285 GHz in Figure 4) can be attributed to small structural modifications around the metal. These slight changes are likely related to the spin transition. Changes in metal−ligand bond lengths accompanying a spin state transition can be obtained from X-ray crystallography. As an example, for Fe^{III} complexes, differences of 0.17 Å can be found for the Fe−N distances but of only 0.04 Å for the Fe−O distances in a series of hexadentate ligands derived from triethylentetramine with a $[N_4O_2]$ donor set.[48]

The rate of the spin-state interconversion for each compound is slower at all temperatures than the EPR time scale (ca. 10^{11} s^{-1}), but chemically fast. At first sight, it seems strange that at these temperatures the reaction rates are fast. In the literature, however, Buhks et al. suggested that dynamics in spin-crossover should be treated as a nonadiabatic process within the theory of radiationless multiphonon relaxation.[49] They predicted that the LS/HS relaxation would be a thermally activated process at elevated temperatures with a nonvanishing tunnelling rate at cryogenic temperatures. Recently, these relaxation rate constants were measured for several Fe^{III} complexes using laser flash photolysis experiments.[50] Two temperature domains were observed. Clearly, the general temperature behaviour consisting of a thermally activated process at elevated temperatures and a tunneling at low temperatures was experimentally observed. Therefore, even at low temperatures, the LS to HS relaxation rate constant remains high. Under these conditions, the equilibrium between the low-spin (LS) and the high-spin (HS) complexes can thus be instantaneously obtained.

Influence of the External Magnetic Field on Spin Crossover

It can be seen from Figure 5 that the critical temperature is also field dependent and T_c increases as the magnetic field increases. To explain this phenomenon, we have treated the spin transition as an equilibrium reaction between two chemical species, the LS and the HS complexes, with x as the molar fraction of the high-spin complex.

$$\begin{array}{lcl} \text{LS} & \leftrightarrows & \text{HS} \\ (1-x) & & x \end{array}$$

Three different situations can be considered:

(i) In the absence of a magnetic field, the molar free enthalpy (Gibbs free energy, G per mol) for this reaction can be written as the weighted sum of the standard free enthalpy ($G_H°$ and $G_L°$) of the pure HS and LS systems in the absence of any cooperative interaction terms, plus two other terms accounting for the mixing entropy (S_{mix}) and the interactions [$I(x)$]:

$$G = xG_H° + (1-x)G_L° - T\,S_{mix} + I(x) \quad (1)$$

If a regular solution of molecules is assumed for the two states, the mixing entropy S_{mix} for the mixing of the chemical species, according to Guggenheim is:[51]

$$S_{mix} = -R[x\ln x + (1-x)\ln(1-x)] \quad (2)$$

The interaction term can be treated by following a model initially introduced by Slichter, then later modified by König and revisited by Kahn, as:[52−54]

$$I(x) = \gamma_{LL}(1-x)^2 + 2\gamma_{LH}(1-x)x + \gamma_{HH}x^2 \quad (3)$$

where γ_{LL}, γ_{LH} and γ_{HH} are pair interaction terms between two LS ions, a LS and a HS pair, and two HS ions, respectively. These terms are likely related to the magnetoelastic coupling between each cell of the two types of spin (mean field approximation). For convenience, $I(x)$ can be rewritten as:

$$I(x) = \gamma_0 + \gamma_1 x + \gamma_2 x^2 \quad (4)$$

with $\gamma_0 = \gamma_{LL}$, $\gamma_1 = 2(\gamma_{LH} - \gamma_{LL})$ and $\gamma_2 = \gamma_{LL} - 2\gamma_{LH} + \gamma_{HH}$.[52−54] If we introduce equilibrium conditions, the differentiation of the free enthalpy as a function of the molar fraction of the high-spin species gives the following equation:

$$\partial G/\partial x = 0 = \Delta G° + \gamma_1 + 2\gamma_2 x + RT\ln[x/(1-x)] \quad (5)$$

where $\Delta G° = G_H° - G_L°$ is the molar standard free enthalpy of the reaction. This expression gives the equilibrium molar fraction x as a function of temperature with $\Delta G° = \Delta H° - T\Delta S°$ where $\Delta H°$ and $\Delta S°$ are the standard molar enthalpy and entropy of the equilibrium reaction, respectively. $\Delta S°$ for the reaction is positive and is much larger than the entropy variation associated with the mere change of spin state, i.e. $R[x\ln(2S_H + 1) + (1-x)\ln(2S_L + 1)] = R\ln(3) = 9.1$ $J\cdot K^{-1}\cdot mol^{-1}$, where S_H and S_L are the total spin value of the high-spin and low-spin states, respectively.

We now defined the critical temperature of the spin-transition in the absence of an external magnetic field $T_c(0)$, from this equation, for $x = 0.5$:

$$T_c(0) = (\Delta H° + \gamma_1 + \gamma_2)/\Delta S\Theta \quad (6)$$

(ii) The application of a static magnetic field, B, to this sample can be described by adding into Equation (1) a Zeeman energy term ΔG_Z ($= -MB/2$). The total magnetisation is the weighted sum of the magnetisation of the two paramagnetic species as:

$$M = x\chi_H B + (1-x)\chi_L B = [\chi_L + x\Delta\chi)]B = [C_L + x\Delta C]B/T \quad (7)$$

where χ_L and χ_H are the high-spin and low-spin susceptibilities and $\Delta\chi = \chi_H - \chi_L$ and $\Delta C = C_H - C_L$. In this last term, C_H and C_L represent the Curie constants of the two species ($\chi = C/T$).

The Zeeman energy term follows as:

$$\Delta G_Z = -[C_L + x\,\Delta C]B^2/2T \quad (8)$$

With this added term, the equilibrium Equation (5) becomes:

$$\partial G/\partial x = 0 = \Delta G° + \gamma_1 + 2\gamma_2 x + RT\ln[x/(1-x)] - (\Delta C/2T)B^2 \quad (9)$$

For $x = 0.5$, the critical temperature of the spin-transition, T_c, is now field-dependent, according to:

$$(\partial G/\partial x)_{x=0.5} = \Delta H^\circ - T_c\Delta S^\circ + \gamma_1 + \gamma_2 - (\Delta C/2T_c)B^2 = 0 \quad (10)$$

giving two solutions (see appendix): (a) one around $T_c(0)$ $T_c = T_c(0) - a'B^2$ with

$$a' = [\Delta C/(2T_c(0)\Delta S^\circ)] \quad (11)$$

This model predicts a parabolic decrease in the critical temperature when the external magnetic field increases. This type of variation has already been observed in good agreement with the predictions for several transition metal ion compounds [$LaCo^{III}O_3$ and $[Fe^{II}(Phen)_2(NCS)_2]$ (Phen: 1,10-phenanthroline)][55−56] and particularly with very high B values from pulsed magnetic fields for $[Fe^{II}(Phen)_2(NCS)_2]$ and $[(Mn^{III}(pyrrol)_3(tren)]$ [pyrrol: pyrrole-2-carboxaldehyde; tren: 2,2′,2′′-tris(ethylamino)-amine)].[57−58] These effects are characterised by a relatively small amplitude (1.5 K from 0 to 23 T). These experiments have been recently reviewed.[59] (b) The other solution gives values at very low temperatures:

$$T_c = a'B^2 \quad (12)$$

This model predicts a parabolic increase in the critical temperature when the external magnetic field increases. However, this effect should be small since a′ is the same coefficient as in Equation (11). In our experiments, however, no such phenomena were observed. In our systems, the variation in the T_c value of the spin-transition as a function of the external magnetic field B is completely different. Instead of becoming saturated, at very low temperature, we found a relatively large and almost linear dependence and as shown in SI2 (Supporting Information; 7.5 K from 3.4 to 10.2 T). The main discrepancy is that Equation (12) is related to a transition between high-spin and low-spin states which is contrary to our observations (always a low-spin state at low temperatures for each field). This behaviour cannot be understood in terms of the framework of the model given above even through the pair interactions γ_{LL}, γ_{LH} and γ_{HH}.

In order to interpret our results we introduced another effect, namely the magnetoelastic coupling associated with low-spin and high-spin volume anomalies.

(iii) We now take into account a magnetoelastic term, according to which the local moment is coupled to the volume of each coordination sphere leading to the fact that the magnetoelastic term of a low spin is different from that of a high spin. The free energy related to this magnetoelasticity for a chemical species can be shown to be proportional to $(\delta V/V_o)$ and M^2 as:[60]

$$\Delta G_{ms} = k_{ms}(\delta V/V_o)M^2 \quad (13)$$

where $\delta V/V_o$ (noted below as ε) represents the relative variation of volume between the ordered and disordered states (also called anomaly of volume), M is the magnetisation in the external magnetic field and k_{ms} is a constant. This is a local coupling which does not imply a cooperative mechanism. In our case, we have a mixture of two species and the total free energy related to the volume anomaly is the weighted sum of the terms of the magnetisation relative to the two species (neglecting the interfacial energies).[54]

$$\Delta G_{ms} = k_{ms}[(1 - x)\varepsilon_L M_L^2 + x\varepsilon_H M_H^2] = k_{ms}[\varepsilon_L C_L^2 + x(\varepsilon_H C_H^2 - \varepsilon_L C_L^2](B/T)^2 \quad (14)$$

with M being $(C/T)B$. By adding this term, Equation (9) becomes:

$$\partial G/\partial x = \Delta G^\circ + \gamma_1 + 2\gamma_2 x + RT[\ln(x/(1 - x)] - (\Delta C/2T)B^2 + k_{ms}[\varepsilon_H C_H^2 - \varepsilon_L C_L^2](B/T)^2 = 0 \quad (15)$$

and $(\partial G/\partial x)_{x=0.5}$ has two solutions for low temperatures (see appendix):

a) field-independent:

$$T_c = 2k_{ms}[\varepsilon_H C_H^2 - \varepsilon_L C_L^2]/\Delta C \quad (16)$$

and b) second-order field-dependent:

$$T_c = \{\Delta C/[2\Delta S^\circ T_c(0)^2] - k_{ms}[\varepsilon_H C_H^2 - \varepsilon_L C_L^2]/[\Delta S^\circ T_c(0)^3]\}B^2 \quad (17)$$

The unknown values of all these parameters prevent further progress at this stage. Nevertheless, it seems that this treatment can be in agreement with the observation of the low-spin state for each field at low temperatures. A more sophisticated treatment is now in progress. The contribution of the magnetoelasticity term in our systems compared with those systems where it was not observed,[55−60] probably originates from the fact that our experiments were performed in frozen solutions as opposed to in the solid-state used in previous studies. Moreover, in our studies, complexes **1** and **2** present very flexible structures because of the nature of the ligands, allowing for the development of volume anomalies.

Conclusion

Our analysis of the HF-EPR spectroscopic data of the two studied complexes has shown that the ZFS parameters strongly depend on the symmetry of the metal ions in the complexes. Conversely, measurements of these ZFS parameters can give information on the symmetry in solution when no other methods give any data. Surprisingly, this work has revealed a spin-crossover (from spin 1/2 to spin 5/2 species) at low temperatures. Another surprise was the observation that the critical temperature of the spin transition was field-dependent but in a somewhat unconven-

tional manner (large positive change instead of small negative one). This phenomenon is likely related to the magnetoelastic properties of the mixture of the two species with their different spin states. Further magnetic studies are in progress to interpret these observations.

Experimental Section

Preparation of the Solutions: Complex **1** was prepared from a 0.1 M aqueous solution of ferric perchlorate [$Fe(ClO_4)_3 \cdot 9H_2O$] (Aldrich) and a 2 M solution of citric acid (Aldrich). The pH was adjusted to 1.95 with sodium hydroxide solution. Complex **2** was prepared from a 0.09 M aqueous solution of ferric perchlorate and a 1.8 M solution of citric acid. The pH was adjusted to 6.25 with sodium hydroxide solution. 1 mL of the respective solution was inserted into an appropriate flask for introduction into the EPR spectrometer.

EPR Instrumentation: High-frequency and high-field EPR spectra were recorded with a laboratory-built spectrometer,[61−62] using frozen solutions. Gunn diodes operating at 95 GHz and equipped with a second and third harmonic generator were used as the radiation source. The high magnetic field was produced by a superconducting magnet (0−12 T). We used a temperature regulation apparatus to maintain the temperature between 4 K and room temperature. Measurements were performed in unsaturated conditions.

Theory for the High-Spin Ferric Ion EPR Spectra

(i) Review of the Spin Hamiltonian for High-Spin Ferric Iron (S = 5/2) in Octahedral Symmetry: This review is given as an introduction to the treatment of the data in the frozen solution state. EPR spectra of paramagnetic complexes under the effect of an external magnetic field and as a function of temperature can adequately be described in the framework of the spin-Hamiltonian parametrisation. This was originally introduced by Abragam and Pryce[63] and then systematically discussed in the book of Abragam and Bleaney.[12] For the high spin iron(III) complexes, the ion ($3d^5$) is in a $^6S_{5/2}$ state. We recall, that in this system with an odd numbers of electrons, at least a twofold degeneracy must remain in the absence of a magnetic field. Thus, the ZFS gives pairs of states (Kramers doublets) related by a time-reversal operator.[12a,64] In EPR experiments, the spin-Hamiltonian therefore has two terms, the Zeeman and the ZFS terms, expressed with the Steven's spin operator equivalents of appropriate symmetry, O_n^m, as:

$$\mathbf{H} = \beta \boldsymbol{B_0 g S} + \sum_{0<n<2S}^{n} \sum_{|m|\leq n}^{m} B_n^m \mathbf{O_n^m} \qquad (18)$$

where B_n^m are parameters to be determined, S is the total electron spin, and n and m are integers with the following constraints: $0 < n < 2S$ (terms with odd n disappear due to time-reversal symmetry)[12a] and the only nonzero terms have $m = lp$ (where l is integral or zero) when the highest rotational symmetry axis is p-fold.[12,65−66] The spin operators O_n^m and the corresponding matrix elements $<M_S|O_n^m|M_{S'}>$ (with M_S, $M_{S'}$ spanning the six values −5/2, −3/2, −1/2, 1/2, 3/2 and 5/2) have been tabulated.[12b] It should be noted that nonzero elements only occur when $|M_S - M_{S'}| = m$ for each $B_n^m O_n^m$ term. The general spin-Hamiltonian for high spin iron(III) can therefore be written as:

$$\mathbf{H} = \beta \boldsymbol{B_0 g S} + B_2^0 \boldsymbol{O_2}^0 + B_2^2 \boldsymbol{O_2}^2 + B_4^0 \boldsymbol{O_4}^0 + B_4^2 \boldsymbol{O_4}^2 + B_4^3 \boldsymbol{O_4}^3 + B_4^4 \boldsymbol{O_4}^4 \qquad (19)$$

The occurrence of the different terms of the ZFS depends on the symmetry around the Fe^{III} centre in the complex. For complexes with pure cubic symmetry, only terms related to $\boldsymbol{O_4}^0$ and $\boldsymbol{O_4}^4$ [12c] occur, as in $Fe^{III}(H_2O)_6$.[67] It will be seen, as in our Fe^{III} citrate system, that the fourth-order terms B_4^m in the spin-Hamiltonian can be neglected and that only the effects of B_2^0 and B_2^2 need to be considered (with the notations $D = B_2^0/3$ and $E = B_2^2$).[68] Under these conditions, the spin-Hamiltonian can be rewritten as:

$$H = \beta B_0 g S + D[\boldsymbol{S_z}^2 - 1/3S(S+1)] + E[\boldsymbol{S_x}^2 - \boldsymbol{S_y}^2] \qquad (20)$$

where D is the axial ZFS and E gauges the rhombic ZFS. For a complex with pure axial symmetry, $E = 0$. When the anisotropy of the Landé tensor g occurs in the same axis as the ZFS, a complete expression of the spin-Hamiltonian for this 6S5/2 state is:

$$H = (G_x/2)[\boldsymbol{S_+} + \boldsymbol{S_-}] - (iG_y/2)[\boldsymbol{S_+} - \boldsymbol{S_-}] + G_z \boldsymbol{S_z} + D[\boldsymbol{S_z}^2 - 1/3S(S+1)] + E/2[\boldsymbol{S_+}^2 + \boldsymbol{S_-}^2] \qquad (21)$$

where $Gq = \beta g_q B_{oq}$, with $q = x$, y or z. The corresponding energy matrix containing 6 × 6 elements $<M_S|H|M_{S'}>$ is shown in Table 1, with $\boldsymbol{z} = G_z + iG_y$ and $\boldsymbol{z^*} = G_z - iG_y$. The locations of $\boldsymbol{S_z}$, $\boldsymbol{S_+}$ (or $\boldsymbol{S_-}$) and $\boldsymbol{S_+^2}$ (or $\boldsymbol{S_-^2}$) are, respectively, the origin of the elements on the diagonal line, on one line above (or under) the diagonal and on two lines above (or under) the diagonal.

(ii) Principle of the Treatment of the Data: The corresponding eigenvalues ε_j and the eigenstates $|\varphi_j>$, with j from 1 to $2S + 1 = 6$, can be obtained by diagonalising the matrix. For the pure axial case, with $E = 0$, two diagonalisations have to be made, one for the orientation according to z, with $z = 0$ (written for this case as a diagonal matrix) and the other, for the orientation according to x or y, with $G_z = 0$ and $z = G_x$. For the rhombic case, where E is different from 0, three diagonalisations have to be made, the first for the orientation according to z, with $z = 0$, the second is made for the orientation according to x, with $G_z = 0$ and $z = G_x$ and the third, for the orientation according to y, with $G_z = 0$ and $z = iG_y$ (diagonalisation of a 6 × 6 matrix with imaginary number elements). In each case, five transitions related to the change of Zeeman level states from −5/2 to −3/2, −3/2 to −1/2, −1/2 to 1/2, 1/2 to 3/2 and 3/2 to 5/2 can be expected. These levels are clearly defined when the Zeeman term is large compared with the ZFS term. For the randomly orientated molecules of the frozen aqueous solutions, the intensity of absorption varies from those parallel to the magnetic field to those perpendicular to the magnetic field (which are more numerous by far). For the axial systems, the perpendicular transitions are only of one type whereas for the rhombic systems, the x and y orientations have to be distinguished. In the axial systems, a qualitative interpretation of the spectra can be made when $g\beta B_o >> D$ (high-field limit). The five ($2S$) permitted M to $M + 1$ transitions between the 6 ($2S + 1$) energy levels can be observed for the following resonance field: $B_r(M) = g_e/g[B_o + (M + 1/2)D']$, where $D' = (3\cos^2\theta - 1)D/(g_e\beta)$ and θ is the angle of the external magnetic field with respect to the main axis of symmetry of the complex.[69] Therefore, when the external magnetic field is parallel to the axis, the neighbouring lines are separated by $2|D|$ and centred at $B_{r//} = g_e B_o/g_{//}$ while they are separated by $|D|$ and centred at $B_{r\perp} = g_e B_o/g_\perp$ when it is perpendicular to the axis.

(iii) Treatment of the Spectroscopic Data for the High-Spin Ferric Ion: In Figure 2, we compare the field location of the transitions

in the experimental spectra with those of the transitions obtained in the energy level diagrams for compound **1**. In the left-hand section (Figure 2, a−d), the experimental spectra are displayed along with the simulations calculated using the program available from Weihe et al.[70] The same simulations can be obtained when the X-Sophe software from Bruker is used.[71] Marks have been added to point out the pure z transitions centred at $B_{0//} = \nu_0/\beta g_{//}$ and the pure x, y transitions centred at $B_{0\perp} = \nu_0/\beta g_{\perp}$. In the right-hand section (e−f in Figure 2), we show the energy level diagrams as a function of the product $g\beta B_0$ in cm^{-1} and the allowed $\Delta M_s = \pm 1$ transitions for the zero-field splitting parameter, D, obtained above. The same type of information is given for compound **2** in Figure SI1 (Supporting Information). These diagrams show the energy value (in cm^{-1}) as a function of $G_q = g_q\beta B_o$ with q for x, y or z (G in cm^{-1}). These energy values are eigenvalues of the energy matrix reported in Table 1. The diagonalisations of the real or imaginary, hermitian and symmetric 6×6 matrices were carried out using the Jacobi method, as described in "Numerical Recipes in Fortran"[72] and using the C programming language with a Linux System. We tried several values for the D and E parameters. The segments related to the five transitions according to the parallel or perpendicular axis for axial systems (e−f in Figure 1) or those related to the five transitions according to the x, y or z axis for rhombic systems (Figure SI 1, Supporting Information) were calculated using Mathmab for each frequency (9.507, 6.338 and 3.169 cm^{-1} related to the 285, 190 and 95 GHz measurement frequencies, respectively). The field positions of these calculated transitions are reported in Figure 2 (a−d) under each experimental spectrum taking into account the $g_{//}$ and $g_{\perp}$ values for the axial systems and in Figure SI1 (Supporting Information) with the g_x, g_y and g_z values for the rhombic systems. These g_q values were evaluated from the field positions of the centres of the set of the five transitions related to each orientation relative to the field. With a negative value of D, in the axial system, Figure 2 (e−f) show that the parallel transition from the lowest level ($M_s = -5/2$) can be observed at low field compared with the centre of the set of the five parallel transitions whereas the perpendicular one is at high field. The agreement seems to be satisfactory both for the field positions and for the evolution of the intensities of the transitions as a function of the temperature.

Appendix

(i) Equation (10) can be resolved as a second order equation with $u = T_c/T_c(0)$:

$(\partial G/\partial x)_{x=0.5} = u^2 - u + a = 0$

with $a = (\Delta C/2\Delta S^\circ)[B/T_c(0)]^2$. The general solution is $u = [1 \pm (1 - 4a)^{1/2}]/2$. The solution for T_c around $T_c(0)$ is, with sign "+" for $\pm$, $u = 1 - a$, i.e.:

$T_c = T_c(0) - a'B^2$
with $a' = (\Delta C/[2T_c(0)\Delta S^\circ)]$.

The second solution, for very low temperatures (sign "−" for $\pm$), is $u = a$, i.e. with the same coefficient a':

$T_c = a'B^2$

(ii) Equation (15) can be resolved as a third-order equation with $u = T_c/T_c(0)$:

$(\partial G/\partial x)_{x=0.5} = u^3 - u^2 + bu - c = 0$

with $b = b'B^2$, $b' = \Delta C/[2\Delta S^\circ T_c(0)^2]$ and $c = c'B^2$, $c' = k_{ms}[\varepsilon_H C_H{}^2 - \varepsilon_L C_L{}^2]/(\Delta S^\circ T_c(0)^3]$.
At low temperatures, around 0 K, i.e. and with $u = \varepsilon$, we obtain the solution for the first-order treatment:

$u = c'/b' = 2k_{ms}[\varepsilon_H C_H{}^2 - \varepsilon_L C_L{}^2]/[\Delta C T_c(0)]$

and for the second-order treatment, the only likely solution is:

$u = (c' - b')\ B^2$

Supporting Information (see also footnote on the first page of this article): Figure SI1 shows simulated and experimental 285 GHz HF-EPR spectra of compound **2** recorded at 60 K with the assignments of the different transitions presented as well as energy level diagrams. Figure SI2 shows the experimental 285 GHz-EPR spectra of compound **2** recorded between 5 and 30 K. Figure SI3 shows the plot of the observed T_c of the 1/2 to 5/2 spin transition of compound **1** as a function of the field.

Acknowledgments

The authors thank Professor Jean-Louis Pierre for his interest in this study and as the initiator of this research in iron in biology. We thank Dr. Yves Frapart (Chimie et Biochimie Pharmacologiques et Toxicologiques, University of Paris V), Dr. Geneviève Blondin (Institut de Chimie Moléculaire d'Orsay, University of Paris XI) and Dr. P. Höfer (Bruker Industry, Wissembourg) for providing X-Sophe simulations. C. B. thanks Prof. Jean-Paul Bertrandias (Institut de Mathématiqes Appliquées, UJF) and Dr. André Eberhard (Laboratoire Modélisation et Calcul, UJF) for their help with the mathematics and the use of Mathlab software, respectively. C. B. thanks Prof. I. Gautier-Luneau (Laboratoire de Cristallographie, UJF) for discussions on the X-ray data for compounds related to those studied here and for fruitful discussions about the influence of the state of protonation on the geometries of complexes of Fe^{III} and Ga^{III} with organic ligands. C. B. thanks also Prof. Andreas Hauser (Département de Chimie Physique, University of Geneva), Prof. M. Cyrot (Laboratoire Louis Néel, UJF) and Dr. M. Guillot (HMFL) for general fruitful discussions. We thank also the "Centre National de la Recherche Scientifique" for support through the GdR 1879 "Deregulation of Iron Metabolism: Chemistry, Biology and Therapeutics".

[1] J. P. Glusker, *Acc. Chem. Res.* **1980**, *13*, 345−352.
[2] D. C. Crans, in *Metals Ions in Biological Systems: Vanadium and its role in Life* (Eds.: H. Siegel, A. E. Siegel), Marcel Dekker, New York, **1995**, chapter 5, p. 147−209.
[3] S. J. Lippard, J. M. Berg, in *Principles of Bioinorganic Chemistry* University Science Books: Mill Valley, CA, **1994**, chapter 12, p. 352−354.
[4] M. J. Milewska, *Z. Chem.* **1988**, *28*, 204−211.
[5] P. Baret, C. Béguin, H. Boukhalfa, C. Caris, J. P. Laulhère, J. L. Pierre, G. Serratrice, *J. Am. Chem. Soc.* **1995**, *117*, 9760−9761.
[6] G. Serratrice, H. Boukhalfa, C. Béguin, P. Baret, C. Caris, J. L. Pierre, *Inorg. Chem.* **1997**, *36*, 3898−3910.
[7] J. L. Pierre, I. Gautier-Luneau, *Biometals* **2000**, *13*, 91−96.
[8] [8a] R. Crichton, *Inorganic Biochemistry of Iron Metabolism*, 2nd ed., J. Wiley, Chichester, **2001**, chapter 5. [8b] R. Crichton, *Inorganic Biochemistry of Iron Metabolism*, 2nd ed., J. Wiley, Chichester, **2001**, chapter 7. [8c] R. Crichton, *Inorganic Biochemistry of Iron Metabolism*, 2nd ed., J. Wiley, Chichester, **2001**, Figure 5-5.
[9] H. G. Parkes, R. E. Allen, A. Furst, D. R. Blake, M. C. Grootveld, *J. Pharm. Biomed. Anal.* **1991**, *9*, 29−32.
[10] M. Grootveld, J. D. Bell, B. Halliwell, O. I. Aruoma, A. Bomford, P. J. Sadler, *J. Biol. Chem.* **1989**, *264*, 4417−4422.
[11] D. L. Bakkeren, C. M. H. De Jeu-Jaspars, C. Van der Heud, H. G. Van Eijk, *Int. J. Biochem.* **1985**, *17*, 925−930.
[12] [12a] A. Abragam, B. Bleaney, *Electron Paramagnetic Resonance of Transition Ions*, Clarendon Press, Oxford, **1970**, p. 140, or: same authors, French translation by Y. Ayant, E. Belorizky, R. Buisson, Y. Merle d'Aubigné, J. Rosset, P. U. F., Paris, **1971**. [12b] A. Abragam, B. Bleaney, *Electron Paramagnetic Resonance*

of Transition Ions, Clarendon Press, Oxford, **1970**, p. 863, or: same authors, French translation by Y. Ayant, E. Belorizky, R. Buisson, Y. Merle d'Aubigné, J. Rosset, P. U. F., Paris, **1971**.
[12c] A. Abragam, B. Bleaney, *Electron Paramagnetic Resonance of Transition Ions*, Clarendon Press, Oxford, **1970**, p. 142, or: same authors, French translation by Y. Ayant, E. Belorizky, R. Buisson, Y. Merle d'Aubigné, J. Rosset, P. U. F., Paris, **1971**.
[13] I. Gautier-Luneau, C. Merle, D. Phanon, C. Lebrun, F. Biaso, G. Serratrice, J.-L. Pierre, *Chem. Eur. J.*, to be submitted.
[14] Y. Alpert, Y. Couder, J. Tuchendler, H. Thome, *Biochim. Biophys. Acta* **1973**, *322*, 34−38.
[15] A.-L. Barra, A. Caneschi, A. Cornia, F. Fabrizi de Biani, D. Gatteschi, C. Sangregorio, R. Sessoli, L. Sorace, *J. Am. Chem. Soc.* **1999**, *121*, 5302−5310.
[16] D. Collison, A.K. Powell, *Inorg. Chem.* **1990**, *29*, 4735−4746.
[17] G. C. Brackett, P. L. Richards, W. S. Caughey, *J. Chem. Phys.* **1971**, *54*, 4383−4401.
[18] R. D. Dowsing, J. F. Gibson, *J. Chem. Phys.* **1969**, *50*, 294−301.
[19] P. P. Schmidt, A.-L. Barra, K. K. Andersson, *High Frequency EPR: New Frontiers in Biology, Chemistry and Physics, an European Workshop*, St Pierre de Chartreuse, June **2000**.
[20] K. K. Andersson, A.-L. Barra, *Spectrochim. Acta* **2002**, *A58*, 1101−1112.
[21] K. K. Anderson, P. P. Schmidt, B. Katterle, K. R. Strand, A. E. Palmer, S.-K. Lee, E. I. Solomon, A. Gräslund, A.-L. Barra, *J. Biol. Inorg. Chem.* **2003**, *8*, 235−247.
[22] R. Aasa, *J. Chem. Phys.* **1970**, *52*, 3919−3930.
[23] A. J. Simaan, F. Banse, J.-J. Girerd, K. Wieghardt, E. Bill, *Inorg. Chem.* **2001**, *40*, 6538−6540.
[24] L. Duelund, R. Hazell, C. J. McKenzie, L. P. Nielsen, H. Toftlund, *J. Chem. Soc., Dalton Trans.* **2001**, 152−156.
[25] K. S. Doctor, B. J. Gaffney, *Appl. Magn. Reson.* **1996**, *11*, 425−435.
[26] S. Slappendel, G. A. Veldink, J. F. G. Vliegenthart, R. Aasa, B. G. Malmstrom, *Biohim. Biophys. Acta* **1980**, *642*, 30−39.
[27] E. K. Pistorius, B. Axelrod, G. Palmer, *J. Biol. Chem.* **1976**, *251*, 7144−7148.
[28] J. P. Renault, C. Verchère-Béaur, I. Morgenstern-Badarau, F. Yamakura, M. Gerloch, *Inorg. Chem.* **2000**, *39*, 2666−2675.
[29] H.-L. Shyu, H.-H. Wei, G.-H. Lee, Y. Wang, *J. Chem. Soc., Dalton Trans.* **2000**, 915−918.
[30] K. J. Berry, P. E. Clark, K. S. Muray, C. L. Raston, A. H. White, *Inorg. Chem.* **1983**, *22*, 3928−3934.
[31] W. R. Hagen, *Coord. Chem. Rev.* **1999**, *190−192*, 209−229.
[32] G. Feher, P. L. Richards, *in Magnetic Resonance in Biological Systems* (Eds.: A. Ehrenberg, B. G. Malmstöm, T. Vännggain), Pergamon Press, **1967**, p. 141−144.
[33] T. J. Neal, S.-J. Kang, I. Turowska-Tyrk, C. E. Schulz, W. R. Scheidt, *Inorg. Chem.* **2000**, *39*, 872−880.
[34] P. J. M. van Kan, E. van der Horst, E. J. Reijerse, P. van Bentum, W. R. Hagen, *J. Chem. Soc., Faraday Trans.* **1998**, *94*, 2975−2978.
[35] M. Matzapetakis, M. Kourgiantakis, M. Dakanali, C. P. Raptopoulou, A. Terkis, A. Lalatos, T. Kiss, I. Banyai, L. Iordanidis, T. Mavromoutakos, A. Salifoglou, *Inorg. Chem.* **2001**, *40*, 1734−1744.
[36] M. Matzapetakis, C. P. Raptopoulou, A. Tsohos, V. Papaefthymiou, N. Moon, A. Salifoglou, *J. Am. Chem. Soc.* **1998**, *120*, 13266−13267.
[37] H. Yokoi, T. Mitani, Y. Mori, S. Kawata, *Chem. Letters* **1994**, 281−284.
[38] R. B. Martin, *J. Inorg. Biochem.* **1986**, *28*, 181−187.
[39] I. Gautier-Luneau, personal communication.
[40] J.-J. Girerd, G. C. Papaefthymiou, A. D. Watson, E. Gamp, K. S. Hagen, N. Edelstein, R. B. Frankel, R. H. Holm, *J. Am. Chem. Soc.* **1984**, *106*, 5941−5947.
[41] P. J. van Konningsbruggen, Y. Maeda, H. Oshio, *Top. Curr. Chem.* **2004**, *233*, 259−324.
[42] A. A. Adimado, *Polyhedron* **1983**, *2*, 1059−1063.
[43] P. Gütlich, H. A. Goodwin, *Top. Curr. Chem.* **2004**, *233*, 3−47.
[44] L. Cambi, A. Cagnasso, *Atti Accad. Naz. Lincei* **1931**, *13*, 809−813.
[45] W. R. Scheidt, C. A. Reed, *Chem. Rev.* **1981**, *81*, 543−555.
[46] M. M. Bhadbhade, D. Srinivas, *Polyhedron* **1998**, *17*, 2699−2711.
[47] C. Brewer, G. Brewer, C. Luckett, G. S. Marbury, C. Viragh, A. M. Beatty, W. R. Scheidt, *Inorg. Chem.* **2004**, *43*, 2402−2415.
[48] E. König, in *Structure and Bonding*, Springer, Berlin **1991**, vol. 76, p. 53−152.
[49] E. Buchks, G. Navoon, M. Bixon, J. Jortner, *J. Am. Chem. Soc.* **1980**, *102*, 2918−2923.
[50] S. Schenker, A. Hauser, R. M. Dyson, *Inorg. Chem.* **1996**, *35*, 4676−4682.
[51] E. A. Guggenheim, in *Mixtures*, Oxford University Press, London, **1952**.
[52] C. P. Slichter, H. G. Drickamer, *J. Chem. Phys.* **1972**, *56*, 2142−2160.
[53] R. Zimmerman, E. König, *J. Phys. Chem. Solids* **1977**, *38*, 779−788.
[54] O. Kahn, in *Molecular Magnetism*, Wiley-VCH, Weinheim **1993**, p. 53.
[55] R. A. Bari, J. Sivardière, *Phys. Rev. B.* **1972**, *5*, 4466−4471.
[56] Y. Qi, E. W. Müller, H. Spiering, P. Gütlich, *Chem. Phys. Lett.* **1983**, *101*, 503−505.
[57] A. Bousseksou, N. Negre, M. Goiran, L. Salmon, J.-P. Tuchagues, M.-L. Boillot, K. Boukheddaden, F. Varret, *Eur. Phys. J. B* **2000**, *13*, 451−456.
[58] Y. Garcia, O. Kahn, J.-P. Ader, A. Buzdin, Y. Meurdesoif, M. Guillot, *Phys. Lett. A* **2000**, *271*, 145−154.
[59] A. Bousseksou, F. Varret, M. Goiran, K. Boukheddaden, J.-P. Tuchagues, *Top. Curr. Chem.* **2004**, *235*, 65−84.
[60] A. Herpin, in *Théorie du magnétisme*, PUF, Paris **1968**, p. 264.
[61] A.-L. Barra, J.-C. Brunel, J.-B. Robert, *J. Chem. Phys. Lett.* **1990**, *165*, 107−115.
[62] F. Muller, M. A. Hopkins, N. Coron, M. Grynderg, L.-C. Brunel, G. Martinez, *Rev. Sci. Instrum.* **1989**, *60*, 3681−3984.
[63] A. Abragam, M. H. L. Pryce, *Proc. Roy. Soc. (London)* **1951**, *205A*, 135−153.
[64] J. S. Griffith, *The Theory of Transition-Metal Ions*, University Press, Cambridge, **1961**, p. 205.
[65] W. Weltner Jr., *Magnetic Atoms and Molecules*, Dover, New York, **1983**.
[66] R. Bramley, S. J. Strach, *Chem. Rev.* **1983**, *83*, 49−82.
[67] C. Béguin, unpublished results.
[68] A. X. Trautwein, E. Bill, E. L. Boominaar, H. Winkler, in *Structure and Bonding*, Springer, Berlin **1991**, vol. 78, p. 1−95.
[69] A.-L. Barra, L.-C. Brunel, D. Gatteschi, L. Pardi, R. Sessoli, *Acc. Chem. Res.* **1998**, *31*, 460−466.
[70] *SIM*, by H. Weihe, Department of Chemistry, University of Copenhagen: J. Glerup, H. Weihe, *Acta Chem. Scand.* **1991**, *45*, 444−448.
[71] M. Griffin, A. Muys, C. Noble, D. Wang, C. Eldershaw, K.E. Gates, K. Burrage, G. R. Hanson, *Molec. Phys. Reports* **1999**, *26*, 60−84.
[72] W. H. Press, S. A. Teukolsky, W. T. Vetterburg, B. P. Flanning, *Numerical Recipes in Fortran: this Art of Scientific Computing*, Cambridge University Press, Cambridge, **1992**.

Received May 19, 2004
Early View Article
Published Online December 6, 2004

